Frontiers in Bioscience Landmark

Front. Biosci. (Landmark Ed) **2025**; 30(4): 36583
https://doi.org/10.31083/FBL36583

Original Research

TMC5 as a Marker of Tumor-Associated Telocytes in Hepatocellular Carcinoma

Ying Xu[1,*], Jing Yu[2,*]

[1]Department of General Surgery, Shandong Provincial Third Hospital, Shandong University, 250031 Jinan, Shandong, China
[2]Department of Pathology, Shandong Provincial Third Hospital, Shandong University, 250031 Jinan, Shandong, China
*Correspondence: xuying2205@126.com (Ying Xu); yujing555666@126.com (Jing Yu)

Academic Editor: Qingping Dou
Submitted: 25 December 2024 Revised: 7 March 2025 Accepted: 19 March 2025 Published: 27 April 2025

Abstract

Background: Tumor-associated telocytes (TATCs) perform a pivotal role in hepatocellular carcinoma (HCC) progression and correlate with poor patient outcomes. This study aims to identify specific markers of TATCs in HCC using single-nucleus RNA sequencing (snRNA-seq) and transcriptomic analyses. **Methods**: Comprehensive snRNA-seq and transcriptomic profiling were performed on HCC and adjacent non-cancerous tissues to detect differential expressed genes (DEGs) in TATCs. Bioinformatics tools, including STING and Cytoscape software, were employed to analyze protein–protein interactions and hub genes. Immune cell interactions were assessed via ligand-receptor network analysis. **Result**: TATCs constituted 0.35% of cells in HCC tissues, with reduced proportions compared to paracancerous tissues (0.35% vs 8.19%). Hub genes, including *TOP2A* (DNA topoisomerase II alpha), *BUB1B* (BUB1 mitotic checkpoint serine/threonine kinase B), *KIF11* (kinesin family member 11), and *CENPF* (centromere protein F) were identified in telocytes (TCs). Transcriptomics revealed 622 upregulated and 758 downregulated genes in TATCs versus TCs. *TMC5* (transmembrane channel like 5) and *SLC35F3* (solute carrier family 35 member F3) emerged as unique TATCs biomarkers, revealing significant associations with poor overall survival (OS) in HCC patients (HR = 1.499 for *TMC5*; HR = 1.562 for *SLC35F3*). **Conclusion**: *TMC5* and *SLC35F3* are promising biomarkers for TATCs in HCC, warranting further validation to explore their clinical and therapeutic implications.

Keywords: hepatocellular carcinoma; tumor-associated telocytes; transcriptomics; single-nucleus RNA-sequence; hub genes

1. Introduction

In China, a significant type of cancer is primary liver cancer, which encompasses three subtypes: hepatocellular carcinoma (HCC), intrahepatic cholangiocarcinoma (ICC), and mixed hepatocellular carcinoma [1]. For roughly 20–40% of patients who are diagnosed with HCC, surgery may be a viable treatment option, which adds significantly to the complexity managing this disease [1–3]. HCC demonstrates a range of genetic features, with tumor cells showing abnormal alterations in cytogenetics, epigenetics, and transcriptomics. Therefore, investigating the gene sequences can provide fresh perspectives to uncover the molecular mechanisms underlying HCC.

Increasing evidence suggests that advanced techniques such as transcriptomic and proteomic analyses of tissues and organs, along with single-nucleus RNA sequencing (snRNA-seq), can be utilized to unravel the genetic complexities of HCC [4,5]. The integration of these methodologies for assessing HCC heterogeneity is viewed as the most efficient strategy for confirming specific hub genes, identifying new therapeutic targets, and uncovering distinct biomarkers associated with particular cell types, such as telocytes (TCs), which are recognized for their role in cancer tumorigenesis.

TCs, originally identified as interstitial cells of Cajal, are characterized by irregularly shaped cell bodies and elongated filopodia known as telopodes (Tps), which are thought to be crucial for communication between cells [6–8]. TCs that are implicated in the progression and maintenance of various tumors, are considered as tumor-associated telocytes (TATCs). TATCs significantly influence the immune microenvironment by modulating immune cell activity via cytokine release and direct cell interactions [9]. Their involvement in immune regulation and tissue healing positions them as potential targets for therapy, highlighting the necessity for additional studies to exploit their distinctive properties in cancer treatment. Nonetheless, the lack of specific biomarkers within HCC tissue complicates the task of defining TATCs' characteristics. Consequently, our objective was to discover unique markers for TATCs through snRNA-seq, transcriptomic technologies, and *in vitro* methodologies.

2. Materials and Methods

2.1 Samples

In this study, six pairs of cancerous tissues and paracancerous tissues were collected from male patients. The inclusion criteria for patients were as follows: male patients pathologically diagnosed with HCC, aged between 45 and 65 years, classified as Barcelona Clinic Liver Cancer (BCLC) Stage A [10], with no history of smoking or alcohol consumption, and who had not received preoper-

ative radiotherapy or chemotherapy. The exclusion criteria included the presence of other malignant tumors or severe extrahepatic diseases. Two seasoned pathologists diagnosed these samples by relying on the rapid freezing pathology results obtained during the surgical procedure. A sample had a volume of 1 mm^3 (>200 mg) to meet the criteria necessary for transcriptomics analysis and snRNA sequence. The para-cancerous tissue was collected by cutting at least 2 cm from the margin of the corresponding tumor. This study received approval from the Ethics Committee of Shandong University affiliated Shandong Provincial Third Hospital (No. KYLL-2024044; https://www.medicalresearch.org.cn/), and informed consent was acquired from the patients. They have been performed according to the Declaration of Helsinki.

2.2 Cell Lines and Co-Cultured Scheme

The MHCC97-H cell line was purchased from Zhongqiaoxinzhou Company of China (ZQ0020, Shanghai, China) and cultured in dulbecco's modified eagle medium (DMEM, ZQ-122, Zqxzh-Bio, Suzhou, China) at 37 °C in a 5% CO_2 incubator. All cell lines were validated by short tandem repeat (STR) profiling and tested negative for Mycoplasma (MycoAlert™ kit; LT07-318; Merck KGaA, Darmstadt, German). The primary TCs were carefully dissected from fresh liver tumor tissues under sterile conditions. Minimized the inclusion of fat and cut tissues into tiny pieces (~1 mm^3) by surgical scissors, then digested them by dissolving collagenase (0.5 mg/mL, 2593923, BioMart, Shanghai, China), dispase II (2.4 U/mL, 40104ES60, BioMart, Shanghai, China), and DNase I (20 µg/mL, ALH044-DLW, Beijing Baiaoleibo Technology Co., Ltd., Beijing, China) in sterile PBS for one minute and filtered the suspension through a 55 µm cell strainer to remove undigested debris. Centrifuged the cell suspension at 300 ×g for 5 minutes to pellet the cells and cultured successfully by the complete medium (ZQ-121, Zhongqiaoxinzhou Company, Suzhou, China) for 48 hours. Collect the non-adherent cells which are more enriched in TCs into a new dish and incubated in a humidified incubator with 5% CO_2 at 37 °C. Then, CD34 (No130-097-418, Guiechem, Xian, China) and CD31 immunomagnetic beads (130-097-047, Nuowei company, Beijing, China) were used to separate the TCs from perithelial and epithelial cells, and TCs were selected successfully [7,11–13]. The identification of TCs was performed by transmission electron microscope assay and immunofluorescent staining with CD34, PDGFRA, and CD31 according to our previous studies [7,14,15]. The primary TCs were validated by STR profiling and tested negative for Mycoplasma. Moreover, these two cell lines were rechecked out of "Error cells directory" (http://www.cellresource.cn; Procell Life Science & Technology Co., Ltd.). Modified version: Experimental groups were established by co-culturing TCs (1×10^4 cells) alongside HCC cell lines (3×10^5 cells) within double-deck petri dishes. In contrast, the control group involved only TCs that were cultured for 48 hours at 37 °C in a 5% CO_2 incubator using the same ZQ-121 medium. Following this, nucleic acid data from both TCs groups were analyzed through high-throughput gene sequencing technology, and the resulting transcriptomic data were employed for further analysis.

2.3 Single Nucleus RNA Sequence Testing

Samples undergo treatment with a particular enzyme to produce a suspension of cell nuclei. This cell suspension goes through several processing steps: it is initially filtered with a 60 µm filter screen, and then a second filtration is performed using a 40 µm filter screen to improve the removal of cell clusters. Once the reverse transcription step is completed, the emulsions are disrupted, and the barcoded cDNA is extracted, followed by RNA amplification. The amplified cDNA obtained is employed for the creation of a 3′ gene expression library. Within the construction of the library, 50 ng of the amplified cDNA is fragmented, end-repaired, subjected to size selection using SPRIselect beads, and then sequenced on the NovaSeq platform (Berry Genomics Company, Beijing, China) 16 to yield 150 bp paired-end reads. The full-length cDNA is subsequently amplified via PCR to ensure an adequate quantity for library preparation. During the incubation of gel bead in emulsion (GEMs), TruSeq Read 1 (a specific primer sequence for Read 1) is incorporated into the molecules. The following processes of End Repair, A-tailing, Adaptor Ligation, and PCR incorporate P5, P7, a sample index, and TruSeq Read 2 (a specific primer sequence for Read 2) into the mixture. Quality control is performed using Qubit HS quantification and Agilent 2100 Bioanalyzer/Fragment Analyzer 5300, resulting in a final library size of approximately 450 bp. After sequencing and quality assessment, raw reads are demultiplexed and aligned to the reference genome via the 10X Genomics Cell Ranger pipeline [16], utilizing default settings. The Seurat package was used [17,18]. The CellMarker website (http://xteam.xbio.top/CellMarker/) was utilized to guide the classification of cell-types [19]. All raw data was produced by Berry Genomics Corporation (http://www.berrygenomics.com).

2.4 Transcriptomics Technology

After a 48-hour co-culture with HCC cell lines, the TCs cells and those from the control group were gathered. Total RNA extraction from both groups was performed utilizing the R1200 kit from Solarbio, located in Shanghai, China. The RNA underwent qualification and quantification through the following procedures: (1) RNA purity and concentration assessments were carried out using a NanoDrop 2000 (Thermo Fisher Scientific, Waltham, MA, USA); (2) RNA integrity and amount were evaluated with the Agilent 2100/4200 system (Agilent Technologies, Santa Clara, CA, USA). Following the construction of the library,

its concentration was assessed using the Qubit® fluorometer (Thermo Fisher Scientific, Waltham, MA, USA). The precise concentration of the cDNA library was further evaluated through qPCR. The library's size distribution was examined using agarose gel electrophoresis. Initial raw data in FASTQ format was processed with custom Perl scripts. Feature-Count was applied to quantify the reads. Differential expression analysis was performed using EdgeR (Walter and Eliza Hall Institute of Medical Research, Parkville, VIC, Australia), with *p*-values adjusted via the Benjamini and Hochberg method to control for the false discovery rate. Genes exhibiting $|\log2\ (\text{FoldChange})| > 1$ and q value < 0.05 were classified as differentially expressed [20,21].

2.5 Electron Microscope

The HCC tissue sample is collected and immediately fixed using a chemical solution (H910607, Haisen Biology company, Hefei, China), to preserve its cellular structures and prevent degradation. Following fixation (Glutaraldehyde, H910607, Hisen company, Shanghai, China), the sample undergoes a series of dehydration steps in graded concentrations of ethanol or acetone to remove all water content. The dehydrated sample is then subjected to critical point drying, a technique that replaces the dehydrant with a liquid that can be transitioned to gas without surface tension effects, preserving the tissue's structure. Next, the dried sample is mounted on a suitable stub to make it conductive and improve electron signal quality. Finally, the prepared sample is placed inside the scanning electron microscope (SEM) (HITACHI, SU9000, Sinaida, Shanghai, China) chamber, and the microscope is adjusted to focus on the area of interest. High-energy electrons are scanned over the surface, and the secondary or backscattered electrons emitted from the sample surface are collected to form a detailed image of tissue's surface morphology, revealing the complex cellular and extracellular structures at high magnification.

2.6 Bioinformatic Analysis

The Cancer Genome Atlas (TCGA)-LIHC database (https://portal.gdc.cancer.gov/projects/TCGA-LIHC), including 424 RNA-seq samples, was used to assess the prognostic values of overall survival (OS), different expression levels with TNM stages, and receiver operating characteristic (ROC) curves of which differential expression genes (DEGs) were screened from snRNA-seq assay. Xiantaoxueshu website was a data visualization software and purchased from Jieluoxuan company of China (https://www.xiantaozi.com/) which could construct heatmap, OS curves, ROC curves, column diagrams and chord diagrams of relationships between DEGs in our study. We utilized the Gene Ontology (GO) database (http://geneontology.org) and the Kyoto Encyclopedia of Genes and Genomes (KEGG) database (https://www.genome.jp/kegg/) [22,23], accessed via Bioconductor (http://www.bioconductor.org/) to explore the signaling pathways associated with the DEGs. For identifying protein-protein interactions (PPI), we used the STRING database (http://string-db.org/), applying an interaction score threshold of >0.4. A confidence score of ≥ 700 was set to determine significance. After downloading PPI data, Cytoscape software (3.9.1 version, https://cytoscape.org) with the CytoHubba plug-in was then used to search and visualize the hub genes with the highest degree of connectivity via MCC algorithms. Correlation analysis, Venn DEGs screening, and heatmap of transcriptomics and snRNA-seq results were screened by limma R package (fgsea and cluster-Profiler plug-in; Walter and Eliza Hall Institute of Medical Research, Parkville, VIC, Australia; https://bioconductor.org/packages/release/bioc/html/limma.html) [24,25], and infiltrated DEGs were next uploaded into Gene Set Enrichment Analysis (GSEA) system to verify enriched pathways shown in our study. The iTALK software (https://github.com/Coolgenome/iTALK) is utilized in the analysis of single-nucleus transcriptomes to evaluate the variances in gene expression of ligands and receptors across different cell types by comparing various samples. Meanwhile, PySCENIC (version 0.12.1; https://scenic.aertslab.org/) identifies modules of co-expression among transcription factors and target genes. It constructs gene mediated networks specific to distinct cell subsets and uncovers critical regulators that uphold cellular characteristics through the area under the curve (AUC)-cell algorithm, which incorporates adjusted values of the Regulon Specificity Score (RSS) [26].

2.7 Statistical Analysis

Comparisons among several groups were performed utilizing one-way analysis of variance (ANOVA), and subsequent post hoc analyses were carried out using Tukey's method. The findings are presented as means $\pm$ standard deviation (SD), with a significance threshold established at $p < 0.05$. Additionally, univariate and multivariate analyses were performed, including Cox proportional hazards regression, to assess the impact of various clinical and pathological factors on overall survival. We also employed ROC curve analysis to determine the diagnostic performance of biomarkers and identify optimal cut-off values. Overall survival was calculated using the Kaplan-Meier method, with differences in survival curves analyzed through the log-rank test.

3. Results

3.1 Overview of Whole snRNA-seq Analysis in HCC and Para-Cancerous Tissues

The snRNA-seq technique was employed to create an extensive representation of the cell clusters present in the tumor microenvironment (Fig. 1). The Loupe browser software, along with Cell Ranger data, was then employed to define the machine clustering outcomes, which indicated the identification of 13 cell clusters within the cancer tis-

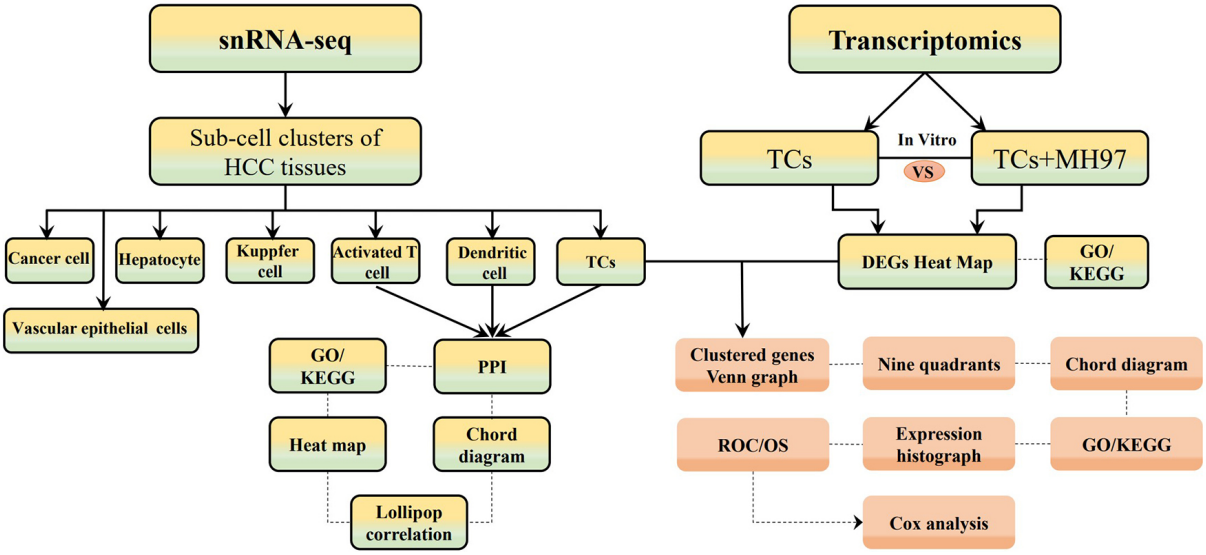

Fig. 1. The flow chart of materials and methods. SnRNA-seq, single nucleus RNA sequencing; HCC, hepatocellular carcinoma; TCs, telocytes; MH97, MHCC97 cells; GO/KEGG, Gene Ontology/Kyoto Encyclopedia of Genes and Genomes; PPI, protein-protein interaction; ROC, receiver operation characteristic curve; OS, overall survival.

sues and 20 clusters in the para-cancerous tissues. These clusters were additionally classified into seven unique subsets for both HCC and the para-cancerous tissues: activated T cells, cancer cells, dendritic cells, Kupfer cells, TCs, vascular endothelial cells, and hepatocytes (Fig. 2A,B,H,I; **Supplementary Fig. 1A**). Remarkably, TCs were identified by employing 25 biomarkers derived from prior study [27] (**Supplementary Table 1**), and the mean frequency of TCs were initially quantified as 0.35% in the HCC tissues (Fig. 2C). The proportion of TCs and Kupfer cells was discerned to be lower in the cancer tissues compared with the para-cancerous tissues (0.35% vs 8.19%; 13.64 vs 18.89%) (Fig. 2C,J). Subsequently, the diverse heatmaps of DEGs in sub-cell populations underscored their heterogeneity in HCC (Fig. 2D–G,K–N; **Supplementary Tables 2,3,4**), and Uniform Manifold Approximation and Projection (UMAP) diagrams along with violin plots of the top 14 DEGs were created (**Supplementary Fig. 1B,C**). To elucidate the functional implications of DEGs, gene ontology and pathway enrichment analyses were conducted using the GO/KEGG browser (**Supplementary Fig. 2**). These analyses revealed that the DEGs were implicated in several signaling pathways including Rap1 (Rap1 orthologs from arthropods), PI3K/AKT, HIF-1 (Hypoxia inducible factor 1), ECM (Multimerin), MAPK, VEGF, and JAK/STAT. These pathways are instrumental in regulating cellular processes such as proliferation, migration, morphogenesis, and angiogenesis. The DEGs in tumor cells were linked to the cell cycle, resistance to platinum-based drugs, the p53 signaling pathway, and the Wnt signaling pathway. These pathways play roles in chromosome segregation, the regulation of the mitotic spindle, and the activity of ATP-dependent microtubule motors.

3.2 Analysis of Cross-Talk Between ATCs and Immune Cells and Regulons

To investigate the intricate interactions between TATCs, immune cells and cancer cells in HCC, we showcased their cluster UMAP graphs for them using the Loupe browser. These graphs indicated that activated T cells were predominant in terms of quantity (Fig. 3A). A comprehensive GO/KEGG analysis showed that the TATCs were closely related with *CD8*$^+$ T cell differentiation, but no clustering information on dendritic cells' behavior with TATCs was obtained (Fig. 3B). Moreover, *TOP2A* (DNA topoisomerase II alpha), *BUB1B* (BUB1 mitotic checkpoint serine/threonine kinase B), *KIF11* (kinesin family member 11), and *CENPF* (centromere protein F) were identified as hub genes of TCs through the use of the String website and Cytoscape software (Spearman's coefficient >0.8; $p < 0.05$), while CD74, the *PRKACB* (protein kinase cAMP-activated catalytic subunit beta) of T cells, *IRF8* (interferon regulatory factor 8), and the *SPI1* (Spi-1 proto-oncogene) of dendritic cells were also highlighted (Fig. 3C–E). The ring heatmap depicted the gene expressions in divergent cell clusters, confirming that TATCs possess unique heterogeneity in their molecular profile compared with immune cells (Fig. 3F). To delve deeper into the cell-to-cell interaction signals that are mediated by these DEGs, we utilized iTALK and PySCENIC software (University of California, San Francisco, CA, USA), renowned for their proficiency in bioinformatics analysis and visualization [28]. Notably, the scatter diagram of regulon activity demonstrated that *E2F8* (E2F transcription factor 8) in TATCs achieved a high Z-score, signifying a crucial role in cell proliferation (Fig. 3G; **Supplementary Table 5**). The visualization analysis demonstrated that the ITGB1 in TCs acts as a crucial

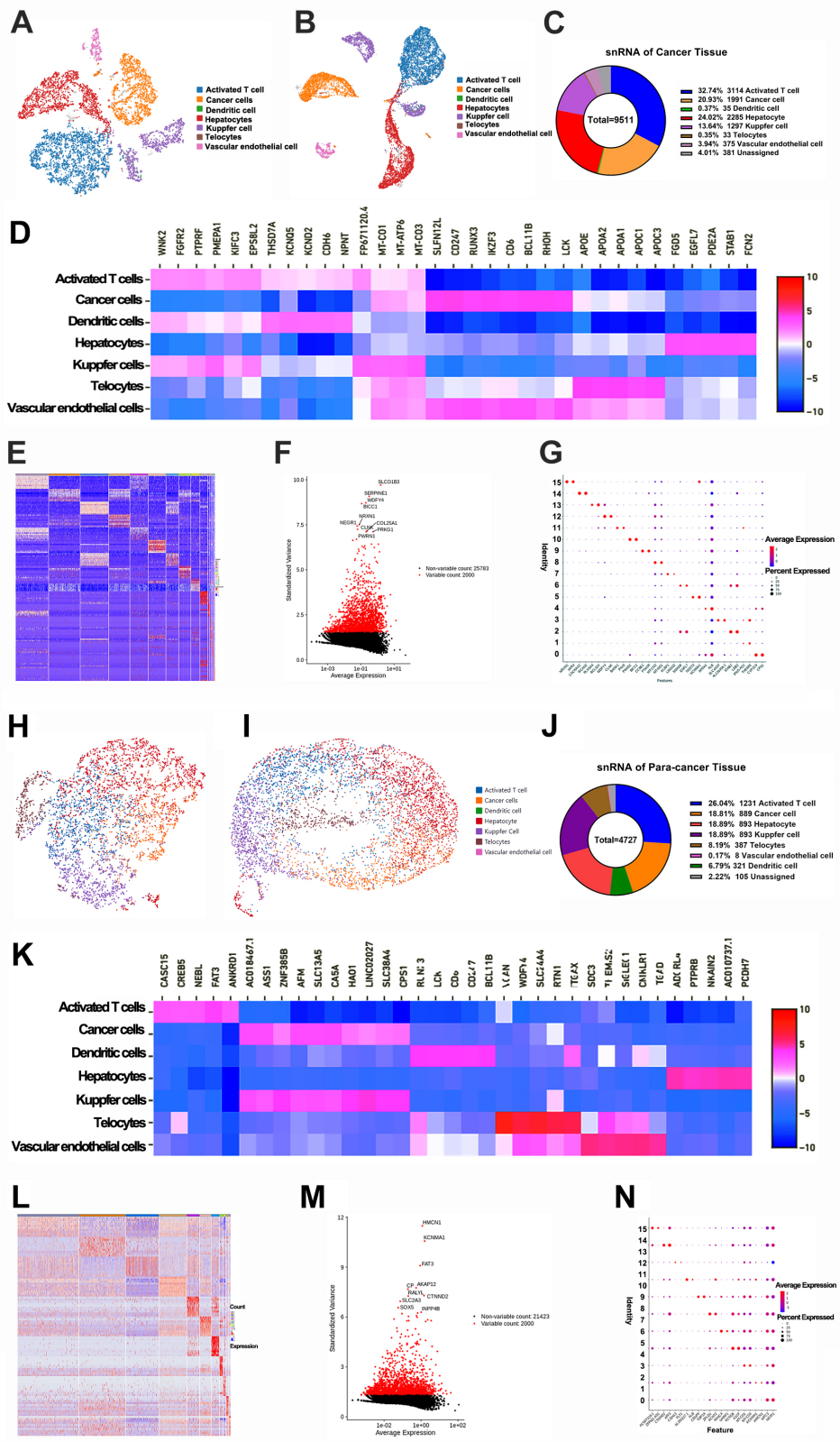

Fig. 2. Analyses of single nucleus RNA sequencing of HCC tissues. (A,B) The UMAP and t-SNE graphs showed sub-cell clusters in HCC tissues. (C) The proportions of sub-cells in HCC tissues. (D,E) The heatmap of DEGs in different sub-cells (Top 35) with Z-scores. (F) The volcano plot of DEGs was screened. (G) The bubble diagram of parts of DEGs with average levels. (H,I) The UMAP and t-SEN graphs showed sub-cell clusters in para-cancerous tissues. (J) The proportions of sub-cells in para-cancerous tissues. (K,L) The heatmap of DEGs in different sub-cells (Top 35) with Z-scores. (M) The volcano plot of DEGs was screened. (N) The bubble diagram of parts of DEGs with average levels. DEGs, differential expressed genes.

receptor for PLG (plasminogen), FN1 (fibronectin 1), and RELN (reelin) within hepatocytes, cancer cells, and vascular endothelial cells. Furthermore, the receptor-ligand interactions revealed molecular communication among cancer cells, vascular endothelial cells, dendritic cells, and TATCs (Fig. 3H). *RRM2* (ribonucleotide reductase regulatory subunit M2) and *KNL1* (kinetochore scaffold 1) emerged as the top two genes in TATCs with Log2FC >2, and the lollipop graph implied a negative correlation of TATCs with dendritic cells, neutrophils, $CD8^+$ T cells, and NK cells, while showing a positive correlation with Th2 cells and T helper cells (Fig. 3I,J). Collectively, the snRNA-seq technique facilitates the distinction of TCs from other cells in the tumor microenvironment (TME) and delineates their crosstalk with T cells and dendritic cells via regulons and hub genes.

3.3 Transcriptomic Changes in TCs After Being Co-Cultured With MH97 Cell-Line

The scanning electron microscope assay, acknowledged as the optimal method for visualizing TCs in cancer tissues [14], enables the identification of the morphology of TCs and HCC cells, thereby substantiating their associative relationship (Fig. 4A). To mimic the presence of TCs in HCC, we executed *in vitro* experiments employing TCs and the HCC cell line. Following this, we examined the transcriptomics (mRNA) of the TCs and TATCs, uncovering that 622 genes were upregulated while 758 were downregulated in TATCs contrasted to TCs (Fig. 4B; **Supplementary Table 6**). Furthermore, these DEGs were subjected to a GO/KEGG network analysis, demonstrating their involvement in the mechanisms of channel activity, transmembrane transporter activity, and the sensory perception of the channel complex (Fig. 4C; **Supplementary Table 7**). This finding illuminates the direct influence of HCC cancer cells on the genetic modulation of TCs.

3.4 Significant Biomarker Analysis of TATCs

To identify biomarkers of TATCs in HCC, we combined snRNA-seq with transcriptomics data, focusing on the analysis of shared genes. The Venn diagram displayed six co-clustered genes derived from the raw sequencing data: *TMC5* (transmembrane channel-like 5), *KCNQ5* (potassium voltage-gated channel subfamily Q member 5), *ZNF385D* (zinc finger protein 385D), *SNAP91* (synaptosome-associated protein 91), *CRP* (C-reactive protein), and *SLC35F3* (solute carrier family 35 member F3) (Fig. 4D,E). It is worth noting that *TMC5* showed a strong correlation with *CRP*, which is potentially involved in opsonin binding, phosphatidylinositol binding, and regulation of macrophage derived foam cell differentiation (Fig. 4F,G). Further analysis revealed that five out of these six biomarkers demonstrated significant alterations between HCC tissues and adjacent cancer tissues according to the TCGA-LIHC database: *CRP* was expressed at lower levels in tumors, whereas *TMC5* and *ZNF385D* exhibited higher expression levels in tumors, while *KCNQ5*, *SLC35F3*, and *SNAP91* had no divergency in either tumors or adjacent cancer tissues based on the TCGA database (Fig. 4H). However, these significant biomarkers might be deemed insufficient as diagnostic predictors due to their inadequate an AUC values (*ZNF385D* = 0.762; *TMC5* = 0.647; Fig. 4I). Furthermore, the OS curves showed that high levels of *SLC35F3* and *TMC5* in HCC patients were associated with a poor prognosis, while *CRP* and *ZNF385D* had no statistical significance based on the TCGA database (Fig. 4J–N. The univariate Cox regression analyses of *TMC5*, *CRP*, *SLC35F3*, and *ZNF385D* based on detailed information showed that high *TMC5* expression is significantly associated with a poor prognosis (HR = 1.499; 95% CI: 1.059–2.122; $p = 0.023$), as is high *SLC35F3* expression (HR = 1.562; 95% CI: 1.102–2.214; $p = 0.012$) (Table 1). Taking together, although *TMC5* and *SLC35F3* were corelated with OS and considered markers of TCs, *TMC5* is more suitable as a biomarker due to its bigger AUC of the ROC curve.

Table 1. The univariate analysis of *TMC5*, *CRP*, *SLC35F3*, and *ZNF385D* with high and low expressions in HCC tissues from TCGA-database.

Characteristics	Total (N)	Univariate analysis	
		Hazard ratio (95% CI)	*p* value
TMC5	373		
Low	187	Reference	
High	186	1.499 (1.059–2.122)	0.023
CRP	373		
Low	186	Reference	
High	187	1.151 (0.815–1.624)	0.425
SLC35F3	373		
Low	184	Reference	
High	189	1.562 (1.102–2.214)	0.012
ZNF385D	373		
Low	186	Reference	
High	187	1.116 (0.790–1.576)	0.534

4. Discussion

With the progress in model technologies, a variety of methods such as snRNA-seq, scRNA-seq, and transcriptomics have been widely employed to investigate the heterogeneity, tumor formation, and embryonic development of various neoplasms in humans [29]. Notably, we identified distinctions between the DEGs derived from snRNA-seq and transcriptomics data. This indicates that the intricate makeup of diverse cell types within the TME is vital for regulating HCC progression. In contrast to the traditional perspective, which emphasizes cancer cells as the pri-

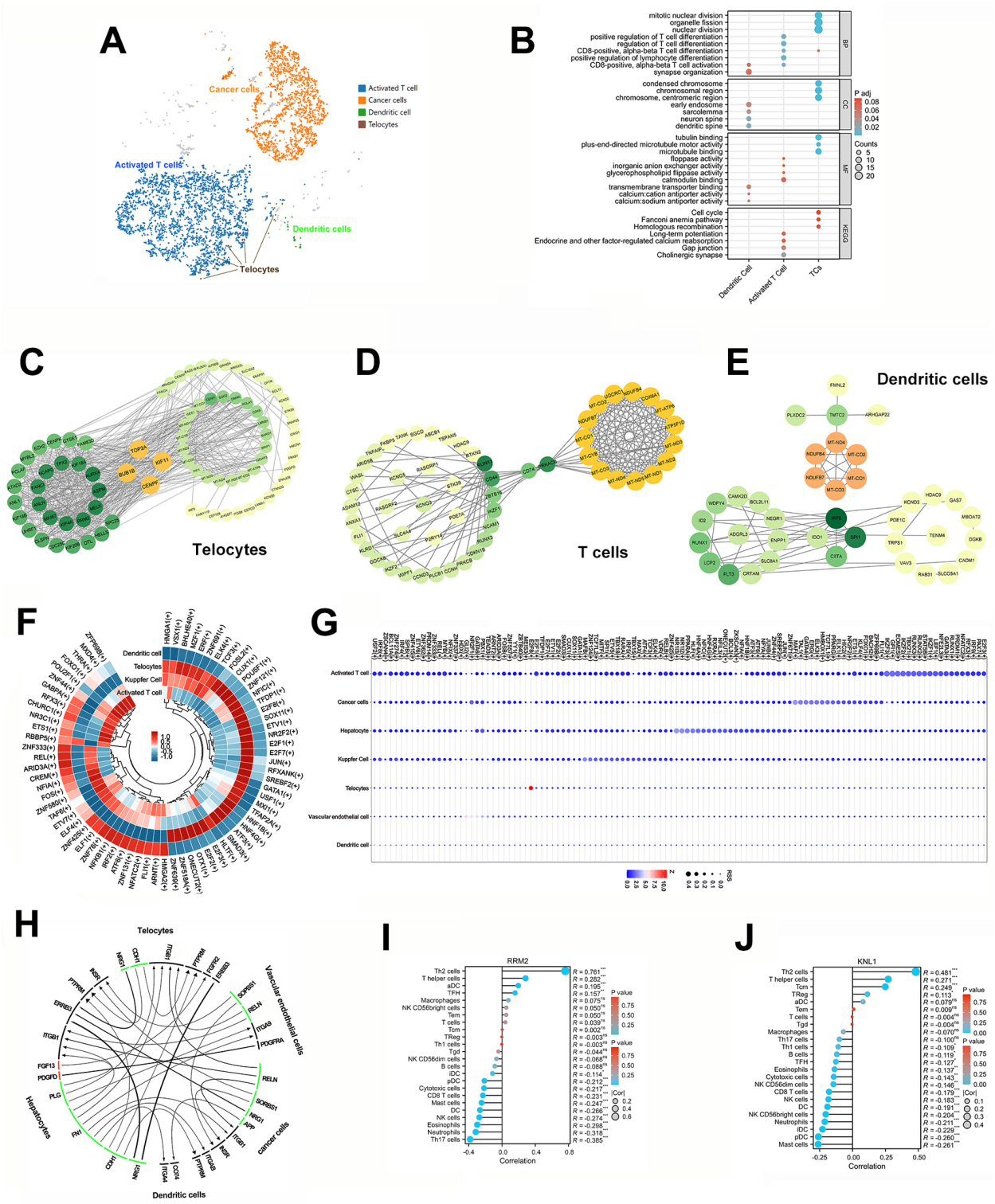

Fig. 3. Bioinformatic analysis of TATCs and immune cells in HCC. (A) The UMAP of T cells, cancer cell, dendritic cell and TCs. (B) GO/KEGG analyses of dendritic cell, activated T cell, and TCs (https://www.kegg.jp/kegg/kegg1.html). (C–E) The protein-protein interactions and hub gene of dendritic cell, activated T cell, and TCs by Cytoscape software. (F) The ring heatmap of DEGs in dendritic cell, activated T cell, Kupfer cell and TCs. (G) The bubble graph of regulons in seven sub-cell clusters with Z-scores. (H) The correlations among sub-cell clusters according to snRNA-seq data by iTALK and PySCENIC software. (I,J) The correlation between TCs and immune cells with top two expression in TCs. $p < 0.05$ as a significant value. *$p < 0.05$, **$p < 0.01$, ***$p < 0.001$, ns > 0.05.

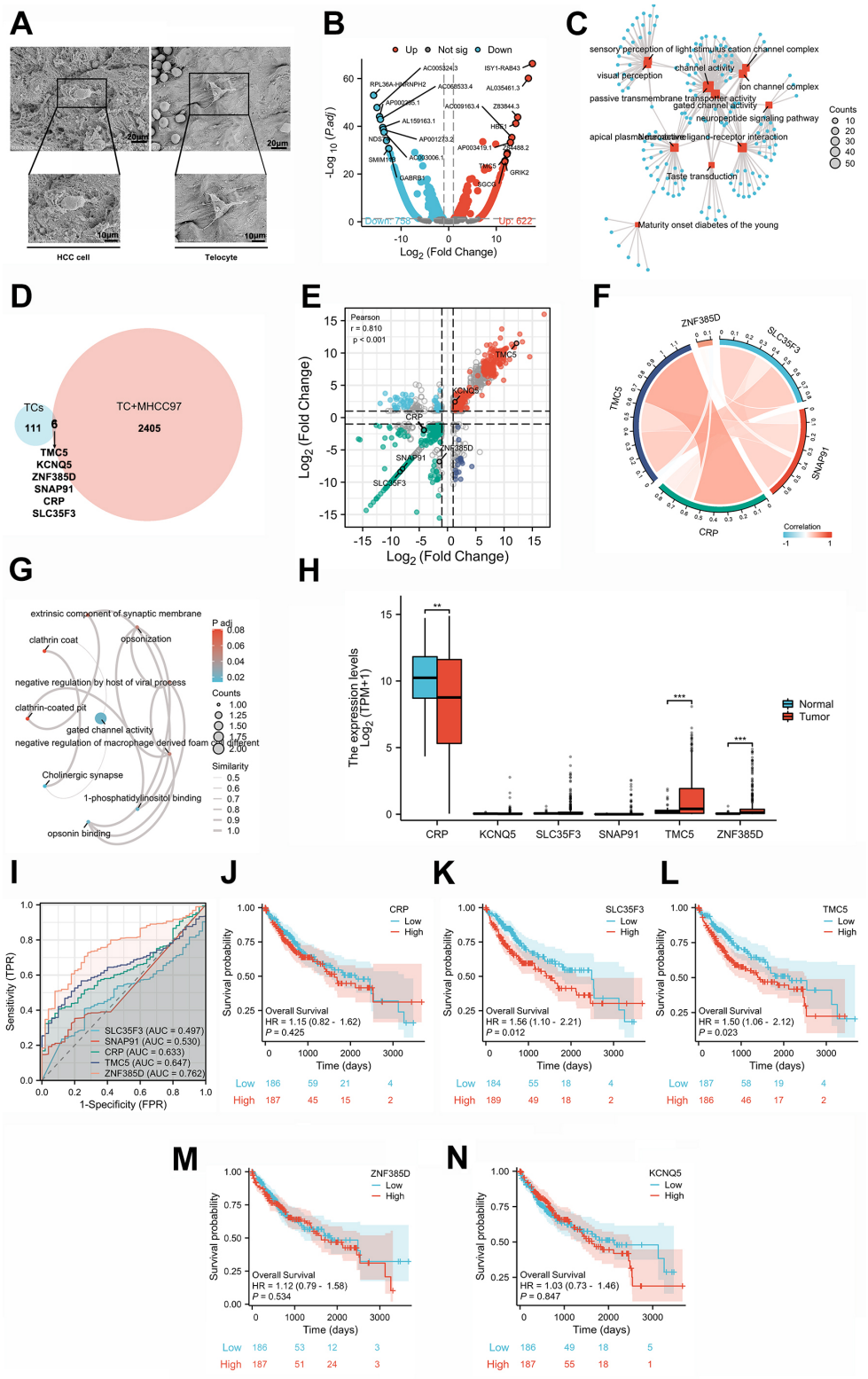

Fig. 4. Transcriptomic changes and clinical significance of TCs after co-cultured with the MH97 cell line. (A) Graphs of HCC cancer cells and TCs under the scanning electron microscope. Scale bars = 10 μm, and 20 μm. (B) The heatmap of DEGs between TCs and TCs co-cultured with MHCC97-H cells. (C) Network chart of DEGs by the GO/KEGG enrichment. (D) The Venn graph of TCs in HCC tissues and TCs co-cultured MH97 cells. (E) Nine quadrants graph of TCs' DEGs from transcriptomic testing and snRNA-seq technology with six co-expression genes. (F) The correlation of six co-expression genes. (G) Network chart of co-expression genes. (H) Expression levels of co-expression genes in HCC tissues and adjacent cancer tissues by TCGA database. (I–N) ROC curves and OS curves of co-expression genes in HCC. $^{**}p < 0.01$, $^{***}p < 0.001$.

mary component, our findings reveal that activated T cells and cancer cells maintain a comparable ratio within HCC tissues. Significantly, this research seeks to quantify the presence of T cells in HCC tissues via snRNA sequencing. This innovative strategy emphasizes the important role of T cells in the TME and underscores the importance of investigating TATCs in the context of HCC. Additionally, T cells engage in extensive interactions with immune cells, suggesting that they could represent a promising new target for immunotherapy in HCC.

TCs represent a specialized subgroup of interstitial cells of Cajal, exhibiting distinct biological functions and immune responses that set them apart from liver fibroblasts, vascular endothelial cells, and stellate cells. Specific biomarkers have been identified for TCs in various organs [13,30–34]. In our previous research, we showed that the expression of MMP9 in TCs was regulated by HCC cells through the secretion of platelet-derived growth factor and exosome-LncRNA SNHG16 [30] to enhance the development and malignant progression of cancer cells. Consequently, we planned an *in vitro* study to explore the transcriptomic alterations of TATCs, which builds upon our theoretical insights into TCs.

Our research indicates that *TMC5* and *SLC35F3* could function as innovative biomarkers of TCs. Recent research has underscored the clinical significance of the *TMC5* gene in various diseases, particularly cancer and metabolic disorders. *TMC5* has been shown to perform a crucial role in modulating the tumor microenvironment and may serve as a prognostic biomarker in HCC by influencing cell proliferation and apoptosis pathways [31]. In colorectal cancer, alterations in *TMC5* expression levels have been correlated with patient outcomes, indicating its potential utility in cancer diagnostics [32]. Additionally, *TMC5* has been implicated in neurodegenerative diseases, where its role in cellular mechanisms related to neuroprotection and neuronal viability is vital [33]. Collectively, these studies highlight the multifunctional nature of *TMC5*, emphasizing its potential as a therapeutic target and biomarker in both cancerous and non-cancerous diseases, thereby paving the way for further investigations into its clinical applications. On the other hand, *SLC35F3*, which is part of the solute carrier family, displays a pivotal role in tumor regulation mainly by facilitating the transport of various molecules through cellular membranes. It is essential in promoting the uptake and metabolism of nutrients, such as sugars or nucleotides, helping to satisfy the increased metabolic requirements of rapidly dividing cancer cells. Furthermore, *SLC35F3* potentially influences cell signaling pathways that govern cell growth, survival, and differentiation, thereby impacting pathways that are commonly dysregulated in cancer, such as growth factor signaling [34]. Although the specific functions of *SLC35F3* in cancer are still under investigation, its involvement in nutrient transport, cellular signaling, modulation of the tumor microenvironment, and possibly in drug resistance underscores its importance within the complex framework of tumor biology [35,36].

Addressing these intricate interactions opens promising avenues for therapy. Possible strategies include interfering with the supportive functions of TATCs, inhibiting immunosuppressive cytokines, and restructuring the extracellular matrix to improve immune cell infiltration. By disrupting the supportive connections between stromal and immune cells within the TME, this strategy aims to boost the effectiveness of cancer immunotherapies. Although our study broadens the understanding of HCC cell clusters and the locations of TCs, it also has certain limitations. Prognostic indicators, such as transcription factors, proto-oncogenes, and oncogenes, require further validation through additional *in vivo* and *in vitro* studies. Moreover, the confirmation of novel biomarkers for TCs in HCC necessitates the examination of a larger cohort of clinical samples.

5. Conclusions

In conclusion, we have identified *TMC5* as a significant marker for TCs, detectable in both cancerous and adjacent healthy tissues via the snRNA sequence technology. This work enhances our understanding of the TME and the heterogeneity of HCC. The current absence of well-defined biological markers for TCs poses challenges in distinguishing them from other stromal cell types. Thus, there is a critical need for innovative strategies to investigate the biology of TATCs.

Availability of Data and Materials

The raw sequence data reported in this paper have been released at https://ngdc.cncb.ac.cn/gsa-human (GSA-Human: HRA006088). The datasets used and/or analyzed during the current study are available from the corresponding author on reasonable request.

Author Contributions

YX, as the first-corresponding author and first author, takes charge of the whole conception and writing of the article. JY, as the second-corresponding author, takes charge of formal analysis, methodology, software, writing-editing. Both authors read and approved the final manuscript. Both authors have participated sufficiently in the work and agreed to be accountable for all aspects of the work.

Ethics Approval and Consent to Participate

The study was carried out in accordance with the guidelines of the Declaration of Helsinki. The study was approved by the ethics committee of Shandong University affiliated Shandong Provincial Third Hospital and could be inquired in Medical Research Registration Information system of China (KYLL-2024044; https://www.medicalresearch.org.cn/), and the written informed consent were signed.

Acknowledgment

We would like to thank Weiwei Meng for the help in revising the English language errors in the manuscript.

Funding

Natural Science Foundation of Shandong Province (ZR2022QH066).

Conflict of Interest

The authors declare no conflict of interest.

Supplementary Material

Supplementary material associated with this article can be found, in the online version, at https://doi.org/10.31083/FBL36583.

References

[1] Mejia JC, Pasko J. Primary Liver Cancers: Intrahepatic Cholangiocarcinoma and Hepatocellular Carcinoma. The Surgical Clinics of North America. 2020; 100: 535–549. https://doi.org/10.1016/j.suc.2020.02.013.

[2] Rumgay H, Arnold M, Ferlay J, Lesi O, Cabasag CJ, Vignat J, *et al*. Global burden of primary liver cancer in 2020 and predictions to 2040. Journal of Hepatology. 2022; 77: 1598–1606. https://doi.org/10.1016/j.jhep.2022.08.021.

[3] Govalan R, Lauzon M, Luu M, Ahn JC, Kosari K, Todo T, *et al*. Comparison of Surgical Resection and Systemic Treatment for Hepatocellular Carcinoma with Vascular Invasion: National Cancer Database Analysis. Liver Cancer. 2021; 10: 407–418. https://doi.org/10.1159/000515554.

[4] Jovic D, Liang X, Zeng H, Lin L, Xu F, Luo Y. Single-cell RNA sequencing technologies and applications: A brief overview. Clinical and Translational Medicine. 2022; 12: e694. https://doi.org/10.1002/ctm2.694.

[5] Vandereyken K, Sifrim A, Thienpont B, Voet T. Methods and applications for single-cell and spatial multi-omics. Nature Reviews. Genetics. 2023; 24: 494–515. https://doi.org/10.1038/s41576-023-00580-2.

[6] Cretoiu SM. Telocytes and Other Interstitial Cells 2.0: From Structure to Function. International Journal of Molecular Sciences. 2022; 23: 16221. https://doi.org/10.3390/ijms232416221.

[7] Faussone Pellegrini MS, Popescu LM. Telocytes. Biomolecular Concepts. 2011; 2: 481–489. https://doi.org/10.1515/BMC.2011.039.

[8] Aleksandrovych V, Gil K. Telocytes in the Tumor Microenvironment. Advances in Experimental Medicine and Biology. 2021; 1329: 205–216. https://doi.org/10.1007/978-3-030-73119-9_11.

[9] Zhang J, Xu Y. Tumor-associated telocytes. Chinese Medical Journal. 2024; 137: 490–492. https://doi.org/10.1097/CM9.0000000000003016.

[10] Bruix J, Reig M, Sherman M. Evidence-Based Diagnosis, Staging, and Treatment of Patients With Hepatocellular Carcinoma. Gastroenterology. 2016; 150: 835–853. https://doi.org/10.1053/j.gastro.2015.12.041.

[11] Zhou J, Zhang Y, Wen X, Cao J, Li D, Lin Q, *et al*. Telocytes accompanying cardiomyocyte in primary culture: two- and three-dimensional culture environment. Journal of Cellular and Molecular Medicine. 2010; 14: 2641–2645. https://doi.org/10.1111/j.1582-4934.2010.01186.x.

[12] Sanches BDA, Maldarine JDS, Tamarindo GH, Da Silva ADT, Lima MLD, Rahal P, *et al*. Explant culture: A relevant tool for the study of telocytes. Cell Biology International. 2020; 44: 2395–2408. https://doi.org/10.1002/cbin.11446.

[13] Romano E, Rosa I, Fioretto BS, Lucattelli E, Innocenti M, Ibba-Manneschi L, *et al*. A Two-Step Immunomagnetic Microbead-Based Method for the Isolation of Human Primary Skin Telocytes/CD34+ Stromal Cells. International Journal of Molecular Sciences. 2020; 21: 5877. https://doi.org/10.3390/ijms21165877.

[14] Wang S, Cheng Y, Liu L, Chen R, Li Y, Wang H, *et al*. The Morphology and Ultrastructure of Dermal Telocytes Characterized by TEM and AFM. Cell Biochemistry and Biophysics. 2024; 82: 705–713. https://doi.org/10.1007/s12013-024-01222-y.

[15] Valente S, Villacampa Lahoz M, Vasuri F, Pasquinelli G. Immunohistochemical and Ultrastructural Characterization of Telocytes in Normal and Diabetic Human Kidneys. Biomolecules. 2024; 14: 968. https://doi.org/10.3390/biom14080968.

[16] Moffitt JR, Hao J, Wang G, Chen KH, Babcock HP, Zhuang X. High-throughput single-cell gene-expression profiling with multiplexed error-robust fluorescence in situ hybridization. Proceedings of the National Academy of Sciences of the United States of America. 2016; 113: 11046–11051. https://doi.org/10.1073/pnas.1612826113.

[17] Zheng GXY, Terry JM, Belgrader P, Ryvkin P, Bent ZW, Wilson R, *et al*. Massively parallel digital transcriptional profiling of single cells. Nature Communications. 2017; 8: 14049. https://doi.org/10.1038/ncomms14049.

[18] Macosko EZ, Basu A, Satija R, Nemesh J, Shekhar K, Goldman M, *et al*. Highly Parallel Genome-wide Expression Profiling of Individual Cells Using Nanoliter Droplets. Cell. 2015; 161: 1202–1214. https://doi.org/10.1016/j.cell.2015.05.002.

[19] Jaitin DA, Kenigsberg E, Keren-Shaul H, Elefant N, Paul F, Zaretsky I, *et al*. Massively parallel single-cell RNA-seq for marker-free decomposition of tissues into cell types. Science. 2014; 343: 776–779. https://doi.org/10.1126/science.1247651.

[20] Wang X, He Y, Zhang Q, Ren X, Zhang Z. Direct Comparative Analyses of 10X Genomics Chromium and Smart-seq2. Genomics, Proteomics & Bioinformatics. 2021; 19: 253–266. https://doi.org/10.1016/j.gpb.2020.02.005.

[21] Batut B, van den Beek M, Doyle MA, Soranzo N. RNA-Seq Data Analysis in Galaxy. Methods in Molecular Biology. 2021; 2284: 367–392. https://doi.org/10.1007/978-1-0716-1307-8_20.

[22] Kanehisa M, Goto S. KEGG: kyoto encyclopedia of genes and genomes. Nucleic Acids Research. 2000; 28: 27–30. https://doi.org/10.1093/nar/28.1.27.

[23] Kanehisa M, Sato Y, Kawashima M, Furumichi M, Tanabe M. KEGG as a reference resource for gene and protein annotation. Nucleic Acids Research. 2016; 44: D457–D462. https://doi.org/10.1093/nar/gkv1070.

[24] Langfelder P, Horvath S. WGCNA: an R package for weighted correlation network analysis. BMC Bioinformatics. 2008; 9: 559. https://doi.org/10.1186/1471-2105-9-559.

[25] Hänzelmann S, Castelo R, Guinney J. GSVA: gene set variation analysis for microarray and RNA-seq data. BMC Bioinformatics. 2013; 14: 7. https://doi.org/10.1186/1471-2105-14-7.

[26] Aibar S, González-Blas CB, Moerman T, Huynh-Thu VA, Imrichova H, Hulselmans G, *et al*. SCENIC: single-cell regulatory network inference and clustering. Nature Methods. 2017; 14: 1083–1086. https://doi.org/10.1038/nmeth.4463.

[27] Xu Y, Tian H, Cheng J, Liang S, Li T, Liu J. Immunohistochemical biomarkers and distribution of telocytes in ApoE$^{-/-}$ mice. Cell Biology International. 2019; 43: 1286–1295. https://doi.org/10.1002/cbin.11128.

[28] Costa-Silva J, Domingues D, Lopes FM. RNA-Seq differential expression analysis: An extended review and a software tool.

PLoS ONE. 2017; 12: e0190152. https://doi.org/10.1371/journal.pone.0190152.

[29] Ahmed AM, Hussein MR. Telocytes in Cutaneous Biology: A Reappraisal. Actas Dermo-Sifiliograficas. 2023; 114: 229–239. https://doi.org/10.1016/j.ad.2022.08.023.

[30] Xu Y, Luan G, Li Z, Liu Z, Qin G, Chu Y. Tumour-derived exosomal lncRNA SNHG16 induces telocytes to promote metastasis of hepatocellular carcinoma via the miR-942-3p/MMP9 axis. Cellular Oncology. 2023; 46: 251–264. https://doi.org/10.1007/s13402-022-00746-w.

[31] Pan L, Fang J, Chen MY, Zhai ST, Zhang B, Jiang ZY, *et al*. Promising key genes associated with tumor microenvironments and prognosis of hepatocellular carcinoma. World Journal of Gastroenterology. 2020; 26: 789–803. https://doi.org/10.3748/wjg.v26.i8.789.

[32] Zhu H, Li Y, Guo J, Feng S, Ge H, Gu C, *et al*. Integrated proteomic and phosphoproteomic analysis for characterization of colorectal cancer. Journal of Proteomics. 2023; 274: 104808. https://doi.org/10.1016/j.jprot.2022.104808.

[33] Song J, Tang Y, Luo X, Shi X, Song F, Ran L. Pan-Cancer Analysis Reveals the Signature of TMC Family of Genes as a Promising Biomarker for Prognosis and Immunotherapeutic Response. Frontiers in Immunology. 2021; 12: 715508. https://doi.org/10.3389/fimmu.2021.715508.

[34] Lee Y, Tjeerdema E, Kling S, Chang N, Hamdoun A. Solute carrier (SLC) expression reveals skeletogenic cell diversity. Developmental Biology. 2023; 503: 68–82. https://doi.org/10.1016/j.ydbio.2023.08.004.

[35] Seo JY, Choi JH. Genetic Variations in Thiamin Transferase *SLC35F3* and the Risk of Hypertension in Koreans. Clinical Nutrition Research. 2021; 10: 140–149. https://doi.org/10.7762/cnr.2021.10.2.140.

[36] Zang XL, Han WQ, Yang FP, Ji KD, Wang JG, Gao PJ, *et al*. Association of a SNP in SLC35F3 Gene with the Risk of Hypertension in a Chinese Han Population. Frontiers in Genetics. 2016; 7: 108. https://doi.org/10.3389/fgene.2016.00108.